

Fractal analysis of geomagnetic data to decipher pre-earthquake process in Andaman-Nicobar region, India

Rahul Prajapati^{1*} and Kusumita Arora¹

¹ Geomagnetism Group, CSIR-National Geophysical Research Institute, Hyderabad-500007, India; rahulphy007@gmail.com

*Correspondence: rahulphy007@gmail.com

Abstract: Seismo-electromagnetic (EM) signatures recorded in geomagnetic data, prior to earthquake, has the potential to reveal pre-earthquake processes in focal zones. The present study analyses the vertical component of geomagnetic field data from Mar 2019 to Apr 2020 using fractal and multifractal approach to identify the EM signatures in Campbell Bay (CBY), a seismically active region of Andaman and Nicobar. The significant enhancements in monofractal dimension and spectrum width components of multifractal highlights the complex nature of the geomagnetic field caused due to interference of high frequency EM emissions during pre-earthquake processes around the West Andaman Fault (WAF) and Andaman Trench (AT) due to micro fracturing and associated deformations. Further, significant enhancements in holder exponents, components of multifractal, highlight the complex nature of geomagnetic field due to interference of less correlated, smooth, and low frequency EM field, indicating that pre-earthquake processes on the Seulimeum Strand (SS) fault may be due to electrokinetic processes. Thus, the monofractal, spectrum width, and holder exponent parameter reveals different nature of pre-earthquake processes which can be identified on an average of 10, 12, and 20 days prior to the moderate earthquakes within a radius of 60 km, which holds promise of short-term earthquake prediction.

Keywords: Geomagnetic; earthquake precursor; Fractal; Andaman-Nicobar

1. Introduction

The existence of precursory signatures prior to an earthquake is a hotly debated topic among researchers across the globe. Several convincing evidences of gas exhalations, variations in groundwater level, temperature variations, fluctuations in the electric and magnetic fields, etc., (Scholz et al., 1973; Rikitake, 1975; Crampin et al., 1980; Bella et al., 1995; Virk et al., 2001; Chadha et al., 2008; Koizumi et al., 2004; Liu et al., 2006; Ouzounov et al., 2007; Panda et al., 1996, 2007; Sethumadhav et al., 2010; Hayakawa and Molchanov, 2004), tilts the scale in favor of detectable signatures of pre-earthquake phenomena. Heterogeneous lithospheric material under strain undergoes micro-fracturing, which causes the polarization of charges, which in turn leads to generation of electromagnetic emission and acousto-gravity waves (Molchanov and Hayakawa, 1995). It has been postulated that most crustal rocks contain dormant electronic charge carriers in the form of peroxy defects, which are released under critical stress levels and flow out of the stressed sub volume as an electric current, which generates magnetic field variations and low frequency EM emissions (Freund and Sornette, 2007). When they reach the Earth's surface, they lead to ionization of air at the ground-air interface (Hayakawa et al., 1996), leading to small disturbances in the local geomagnetic field. Observations of electromagnetic emissions prior to earthquake in frequency ranges from DC, ultra-low frequency, very low frequency, electromagnetic pulses, and very high frequency (Bulusu et al., 2023; Conti et al., 2021; Han et al., 2016; Hattori et al., 2013a; Hayakawa et al., 1999, 1996; Johnston et al., 1984) have been reported by many researchers. Presence of precursory signatures in the ULF range have been extensively studied for earthquakes of $M \geq 7$, such as Biak, Spitak, Loma Prieta, Guam, Chi-Chi, Chiapas etc., (Fraser - Smith et al., 1990; Hattori et al., 2004b; Hayakawa et al., 2000, 1999; Ida et al., 2008; Kopytenko et al., 1993; Molchanov et al., 1992; Smirnova et al., 2013; Stanica and Stănică, 2019; Yen et al., 2004); the ULF range has received more attention as they experience less attenuation and are more likely to reach the Earth's surface and geomagnetic recording station. Hayakawa

et al. (2005) have examined the 3-component data from the same station to identify the anomalous signatures in the polarization ratio of the ULF geomagnetic signal and the diurnal ratio of the Z component for these moderate earthquakes and found a correlatable pattern of these signatures with earthquake occurrence in 75% of the events. This encouraged a deeper investigation into the possible causes of these patterns.

Identification of the geomagnetic anomalies, which are associated with lithospheric processes is a contentious issue. These variations must be uniquely identified, which are distinct from the expressions of magnetospheric-ionospheric processes due to interaction with the solar wind. The most preferred signal processing techniques in previous studies are polarization ratio analysis, diurnal ratio, principal component analysis, singular value decomposition, mono-fractal, and multifractal analysis (Bulusu et al., 2023; Gotoh et al., 2002; Hattori et al., 2004b; Hayakawa et al., 2007, 2005, 1999; Rawat et al., 2016). These signal processing techniques have shown promising results in different cases such as central frequency of 0.01 Hz of non-overlapping window of night time data studied by Han et al. (2015), Hattori et al. (2013b), and Xu et al. (2013), using filtered diurnal signal (using db5 wavelet function) of target station and reference station; Han et al. (2015) have studied diurnal ratio of electric as well as magnetic fields along with polarization ratio of magnetic field of night time data in the ULF range, and Heavlin et al. (2022) studied the signal from a dense network of stations using linear discrimination analysis (LDA) in frequency range 0.001-25 Hz.

The Andaman-Nicobar region lies in the northern part of the Sumatra subduction zone, where the Indian plate is thrusting under the Burma microplate (Gahalaut et al., 2013; Meng et al., 2012; Yang et al., 2017). Persistent tectonic activity is observed here along three major faults, i.e. West Andaman Fault (WAF), Aceh Strands (AS), and Seulimeum Strands (SS). Some of the major earthquakes along these faults have led to

huge losses of life and property and continue to be a worrisome source of mega-scale hazards. During Mar- 71
2019 to Apr-2020, 63 moderate earthquakes of $M \geq 4.5$ occurred in the vicinity of the geomagnetic station 72
installed by CSIR-NGRI at Campbell Bay (CBY) in Great Nicobar (Figure 1). The property of Self 73
Organized Critically (SOC) of earthquakes provides the motivation to study the fractal characteristics of 74
the geomagnetic time series to decipher the nature of the anomalous signatures in the data (Bak et al., 1988; 75
Hayakawa et al., 1999). Nature's behavior in form of biological, physical, geophysical parameters exhibits 76
complex behavior, the details of which can be studied through long range correlations of non-linear patterns. 77
This non-linear behavior exists differently in different field of knowledge such as space plasmas 78
(Szczepaniak et al., 2008; Borovsky and Valdivia, 2018) and earthquakes (Telesca et al., 2005; Rahimi et 79
al., 2022) in geophysical systems and nonlinear waves (Shen and Tian, 2021; Gao et al., 2021) or 80
multifractality (Barabási and Vicsek, 1992; Kantelhardt et al., 2002) in mathematical systems. These natural 81
processes are self critically organized and often follow power law relation, which can facilitate the 82
extraction of information of undergoing processes. The fractal and multifractal formalism in time or space 83
domain has efficacy to delineate the complexity of such natural processes. The concept of fractals is used 84
to characterize the properties of geometrical objects and later introduced to characterize the self-affine time 85
series data following power law behavior (Mandelbrot and Van Neiss, 1968; Dimri, 2005). In recent years, 86
the fractal method has become a popular tool in characterization of complexity of dynamic evolution of 87
several type of natural processes including complex behavior of seismicity. The spatial distribution of 88
earthquakes shows fractal behavior, wherein the fractal dimension can give an idea of heterogeneities of 89
geological compositions and degree of fracturing of rocks (Pasten and Orrego, 2023). Apart from that, 90
fractals also describe the characteristics of seismic events such as frequency, sequence, and time-scale of 91
seismic events, which assist in earthquake forecasting. Fractal method aid the study of the complex nature 92

of Earth system and can be used to extract more insights of seismicity and its relation to tectonic forces 93
(Molchan and Kronrod, 2009; Bhattacharya and Manna., 2007). Fractal method is being applied to study 94
local geomagnetic field patterns in order to comprehend the complex dynamics of crustal caused by 95
impending earthquakes (Gotoh et al., 2004; Currenti et al., 2005; Ida et al., 2005). In the case of the Guam 96
earthquake, 1993, a significant change in scaling exponent prior to the event is found (Hayakawa et al., 97
1999). A similar behavior of scaling exponent was also observed prior to the Biak earthquake in 1996 98
(Hayakawa et al., 2000). Fractal nature is tested with different approaches (Higuchi, 1988); the Higuchi 99
method provides more consistent and reliable fractal dimension value for the study of fractal behavior of 100
ULF signal (Hattori et al., 2004a; Gotoh et al., 2003; Smirnova et al., 2004). Further, multifractal techniques 101
can better represent the different sources of the signals associated with seismicity (Turcotte, 1989). 102

In this study, we will use nighttime Z-component geomagnetic signal as it is more sensitive to changes in 103
local EM emissions, which are likely to be generated by microfracturing and associated lithospheric 104
deformation. We propose to compute the fractal and multifractal dimensions of the data to extract signatures 105
of more intense perturbations of the signal represented by higher fractal dimension values. The anomalous 106
EM emissions can be correlated with earthquake events in search of pre-earthquake signatures. The 107
earthquake catalog (Table T1) of the study region is adopted from the International Seismological Centre 108
(ISC) with $M \geq 4.5$ and epicenter within 250 km radius of recording station. 63 earthquakes are recorded 109
from 31 March 2019 to 24 April 2020. 110

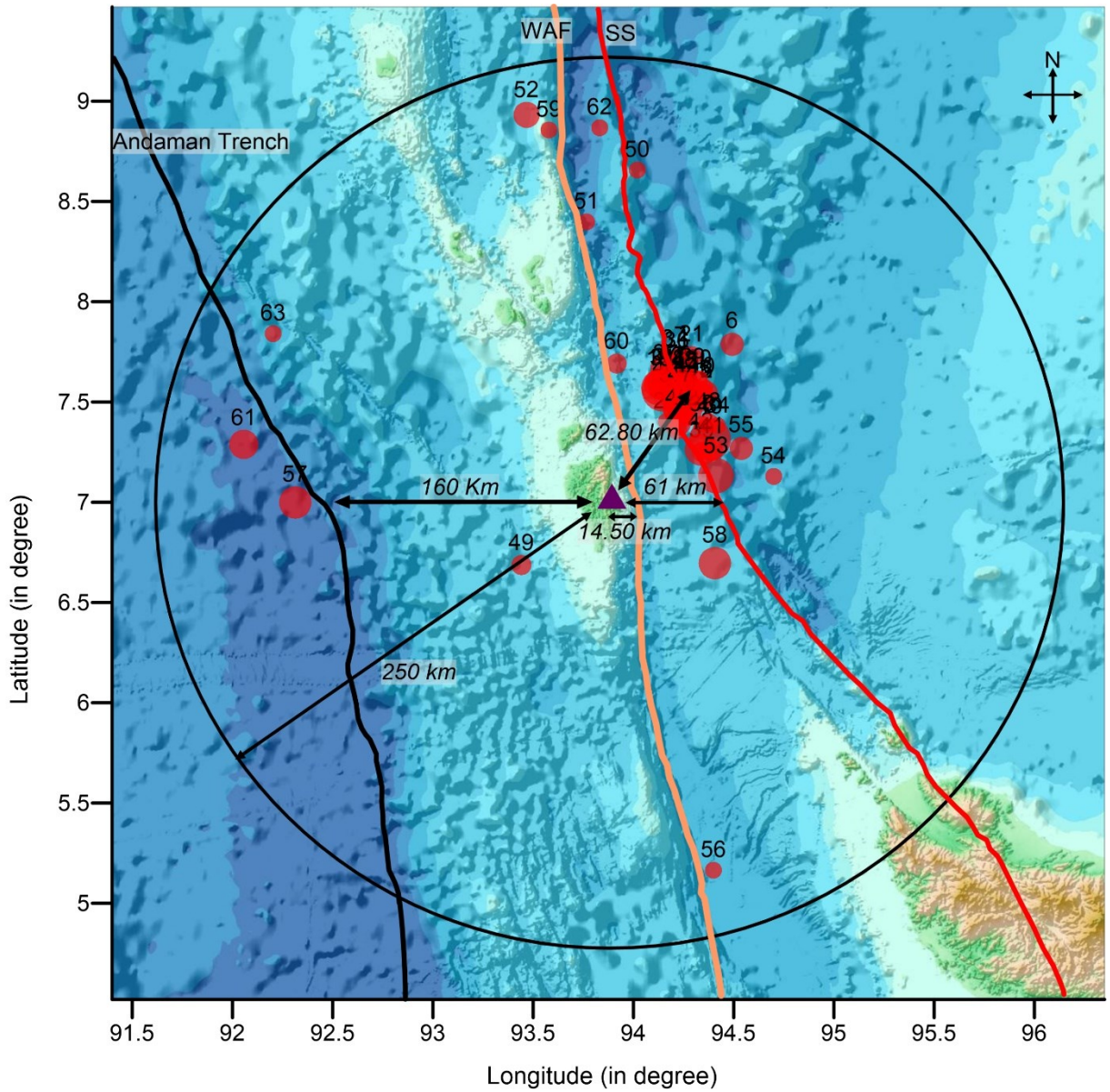


Figure 1. Bathymetry map of Andaman-Nicobar subduction zone including Sumatran Fault System; i.e. Seulimeum Strand, West Andaman Fault and Andaman Trench (modified after Cochran 2010; E. Anusha et al., 2020). The circles are representing the earthquake's location and magnitude (size of circle) correspond to each fault system.

2. Methodological Approach

123

It is proposed to apply both fractal and multifractal approaches to the Z component time series, to distinguish between the different source characteristics and examine their relationship to earthquake parameters. The Z-component of 1 Hz geomagnetic signal analyzed because it is more prone to sense or affected by the local EM field from lithospheric deformation in which vertical components are dominated.

124

125

126

127

- (i) Fractal behavior of Z-component for one-day data using Higuchi is tested and examined. Gotoh et al. (2003) tested different methods for estimation of fractal dimension of geomagnetic signal and suggested that the fractal dimension value using Higuchi method, provided in equation as below, is more reliable and consistent than others. In Higuchi method, a time series $x(n)$ decomposed in to time series of different length x_k^m , defined as:

128

129

130

131

132

$$x_k^m: x(m), x(m+k), x(m+2k), \dots \dots x\left(m + \left(\frac{N-k}{k}\right) \cdot k\right) \quad (i)$$

133

Where, n is $1, 2, 3 \dots N$, m is $1, 2, 3 \dots k$, and k is $1, \dots, k_{max}$. The average length of decomposed time series $L_m(k)$ computed at interval of time from $k = 1$ to k_{max} are related to each other as:

134

135

$$L(k) \propto k^{-f_D} \quad (ii)$$

136

Where, f_D is fractal dimension and equal to the slope of fitted line over $\log(L(k))$ versus $\log(1/k)$.

137

Application of Higuchi method on one day nighttime (22:00-02:00 LT) Z-component of geomagnetic signal of 3 April 2019, is shown in Figure 2.

138

139

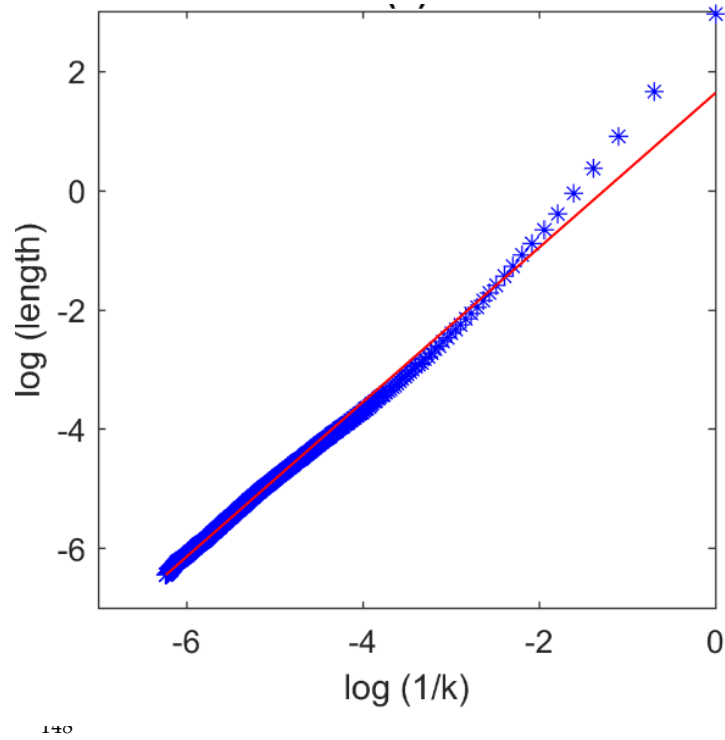


Figure 2. The linear fitting over log of average length and log of size of time interval (scale) showing the power law nature of geomagnetic signal.

(ii) Muzy et al. (1994) proposed an approach for multifractal analysis based on discrete wavelet or wavelet leader. In this approach, the local suprema $f_{i,k}$ obtained from discrete wavelet coefficients (Jaffard et al., 2006; Wendt et al., 2008) at dyadic scales, where, k is translation parameter, i is scale, and the position in time for dyadic interval is $2^i k$. The local suprema of wavelet coefficients $f_{i,k}$ obtained at dyadic scale, assist to compute the multiresolution structure function $S_{xL}(q, i)$ for computation of global holder exponent (Serrano and Figliola, 2009) i.e.

$$S(q, i) \sim (2^i)^{\tau(q)} \quad \text{(iii)}$$

Where, i is scale, q is moment and $\tau(q)$ is scaling exponent. The scaling exponent follows power law relation can be estimated by following relation

$$\tau(q) = \lim_{i \rightarrow 0} \inf \frac{\log(S_{xL}(q, i))}{\log(2^i)} \quad (\text{iv}) \quad 162$$

The spectrum of holder exponent derived from multifractal formalism using legendry function
 which leads to (Serrano and Figliola, 2009). 163
164

$$f(\alpha) = \inf(1 - \tau(q) + \alpha(q) * q) \quad (\text{v}) \quad 165$$

Where α is global holder exponent and $f(\alpha)$ is function of global holder exponent. The degree of
 intermittency or multifractality is defined by multifractal or singularity spectrum i.e. $\Delta \alpha = \alpha_{max} -$
 α_{min} . Larger width of multifractal spectrum indicates larger multifractality or intermittency, and vice-
 versa. The width of multifractal spectrum h_w (from $-q$ to $+q$) indicates the overall degree of
 multifractality of signal. The spectrum width h_{wp} ($q > 0$) and h_{wn} ($q < 0$) indicates the weaker and
 stronger singularity of multifractal signal. The $h_{max}-h_{min}$ curve defines the average fluctuations
 embedded in the signal while $h(0)$ represents the zero-order exponent or monofractal dimension
 (Hayakawa et al., 1999). Similarly, f_{max} define the exponent which occurred maximum number of times.
 Application of multifractal on one-day nighttime (22:00-02:00 LT) Z-component of geomagnetic signal
 of 3 April 2019, is shown in Figure 3. 166
167
168
169
170
171
172
173
174
175

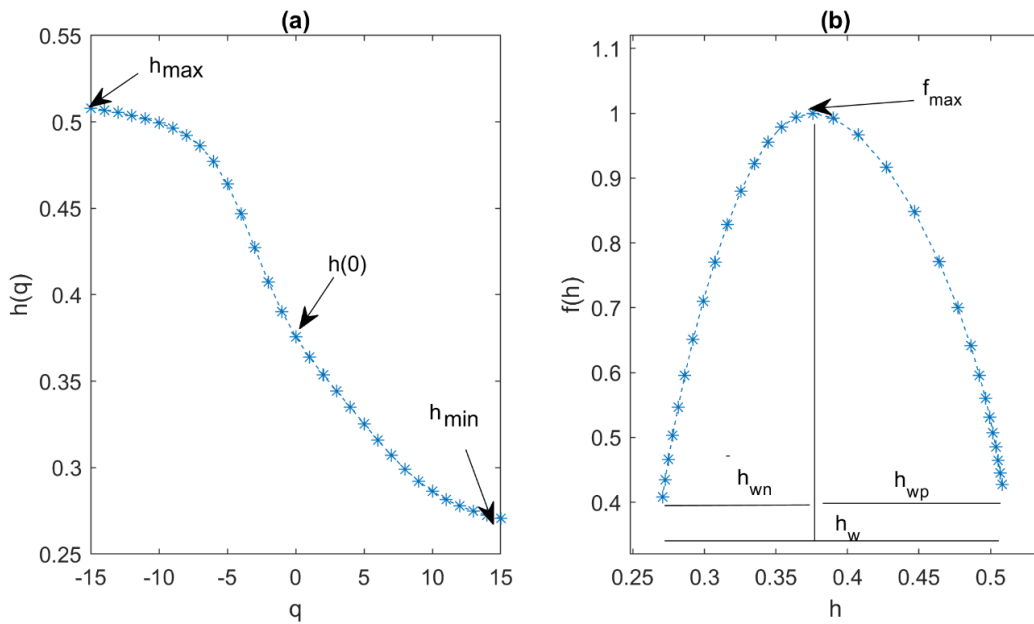


Figure 3. The multifractal analysis for 1800 samples of 3rd April 2019, where (a) The variation of holder exponent (h) with moment order q in range of -15 to +15 showing as h_{min} , h_{max} , and $h(0)$. (b) Multifractal spectrum showing the width of spectrum h_w , h_{wp} and h_{wn} .

- (i) The high correlated values measured from fractal, is reason to select the Higuchi method, while for multifractal, wavelet leader is selected due to compact support for wide range of q ($-q$ to $+q$) and stability for scaling function for negative q values compared to other techniques. From fractal, the power law behaviour, and from multifractal, the finite width of multifractal spectrum and variation in holder exponent indicates the fractal and multifractal nature of signal, respectively.
- (ii) The fractal dimension f_D of the total duration of Z-component data is calculated for consecutive time windows of 30 min to trace the variations of the fractal dimension, producing eight values for each day. The choice of a 30 min time window (consisting of 1800 data points) is based on the balance between the stability of fluctuations in fractal dimension and minimizing loss of information after trials with 15 min and 1 hr. time windows.
- (iii) Similarly, the spectrum width parameter ($h_w, h_{wp},$ and h_{wn}) and holder exponent parameter h_{max} , h_{min} and, $h(0)$ estimated for the total length of Z component from window of 30 minute to identify the degree of singularity or complexity (global, weaker, and stronger) as well as degree of fluctuations with respect to amplitude (from smaller to larger). The shorter fluctuations in fractal dimensions are smoothed by applying a 15-day moving mean.
- (iv) The increments in fractal dimension and multifractal parameter (spectrum width and holder exponent) value greater than the threshold value ($\mu + \sigma$) are considered as a significant increment as evidence of existence of EM signatures from lithospheric deformation.

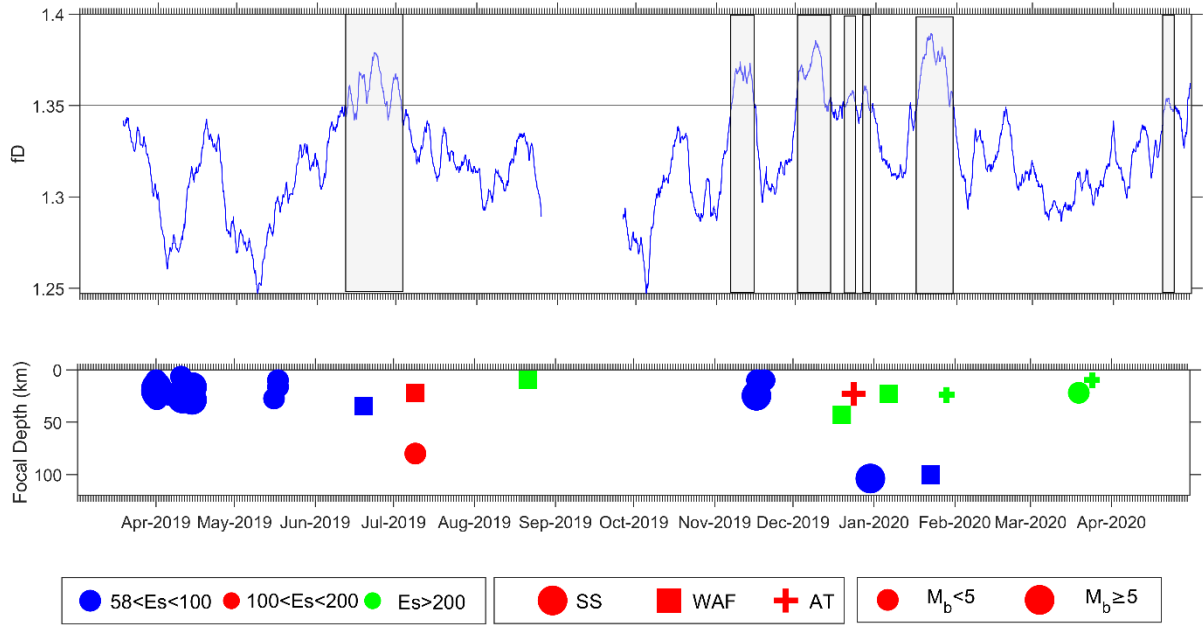
3. Results

207

3.1 Monofractal analysis

208

209



218

Figure 4. (a) Temporal variation of fractal dimension estimated from Higuchi method (15 days moving mean) of Z-component of geomagnetic signal. (b) The time line earthquake occurrences in same duration of geomagnetic signal.

219

220

221

The temporal variations in f_D of vertical component of geomagnetic signal are shown in Figure 4a; f_D greater than the threshold value 1.35 (defined by $\mu + \sigma$) are indicated by grey color rectangles. The increasing fractal dimension values are directly proportional to increasing degree of complexity of signal. A synthetic test (supplementary document) of fractal dimension on fraction Brownian motion signals (fBm) with Hurst exponent 0.2, 0.4, and 0.5 i.e. monofractal signal with increasing degree of complexity (Figure S1) shows higher fractal dimension values (from Higuchi method, Figure S2) for lesser Hurst exponent signal. Moreover, combination of all three signal i.e. multifractal signal shows smaller fractal dimension

222

223

224

225

226

227

228

values indicates that multifractal signal can't be characterized in detail using monofractal dimension. Thus, 229
the observed enhancements in f_D of geomagnetic signal are considered as increasing complexity from EM 230
signatures caused by impending earthquakes. These enhanced values possibly represent the additional 231
complexity in the signal caused by pre-earthquake microfracturing. The temporal location of enhanced 232
fractal dimension values and their correlations with forthcoming earthquakes are summarized in Table T2. 233
For the earthquake swarm of 1-18 Apr, 2019, and the three earthquakes of 16 & 17th May, 2019, no 234
preceding or coinciding enhancements are recorded. Two phases of enhancements during 12-13 and 16-19 235
Jun, 2019 occur prior to earthquake of 19th Jun, 2019 (M=4.6 of focal depth of 35 km, along the WAF with 236
epicentral distance of 60 km). The enhancements during 20-26 Jun, and 29 Jun-2 Jul 2019 occur before the 237
dual earthquakes of 9-Jul, 2019 (M=4.5-fd 80 km-epicenter distance 185 km along SS fault; M=4.5-fd 22 238
km epicenter distance 156 km along WAF). No enhancements beyond threshold value are recorded prior 239
to the very shallow 10 km depth earthquake of 21 Aug (M=4.8) with epicenter 219 km away along the 240
WAF. During Sept and Oct, 2019 neither earthquakes nor enhanced fractal dimensions are observed. Three 241
earthquakes occurred in November, two on 17th and one on the 20th, all on the SS fault. They were of M 242
5.1, 4.5, 4.7 respectively at shallow focal depths and corresponding epicenters at 60, 91, 78 km from 243
recording site. These events are preceded by a long duration enhancement in fractal dimension from 6-15 244
Nov. In December, three earthquakes occurred on 19th, 24th and 30th of magnitudes 4.5, 5, 5 respectively on 245
the WAF, AT and SS faults respectively. The earthquakes of 19th Dec of focal depth 43 km and despite 246
large epicentral distance of 212 km from recording site, was preceded by a large amplitude and long 247
duration enhancement of fractal dimension 1-14 Dec; for the next two earthquakes of focal depths 23 and 248
104 km and corresponding epicentral distances of 173 and 67 km minor enhancements were observed 249
during 18-23 Dec and 26-28 Dec. For the three earthquakes of Jan 2020, the M 4.5 shallow earthquake of 250

6th Jan with epicentral distance >200 km, no enhancements are observed. The earthquakes of 22nd and 28th Jan occurred. No earthquakes were recorded in Feb 2020 and no anomalous enhancements are observed. During March 19th and 24th there were two shallow M=4.5 earthquakes with epicentral distances more than 200 km along the SS and AT respectively. During 20-22 Apr, a small enhancement is observed, the succeeding earthquake is not included in present catalogue.

3.2 Multifractal analysis

The holder exponent curve and multifractal spectrum width are calculated for the same data of 3rd April, 2019 for the 30 min interval 22:00 – 22:30 LT, with 1800 data points. The large variation in Hurst exponent against moment order q (Figure 4a) and wide width of multifractal spectrum of geomagnetic time series (Figure 4b) indicate the multifractal nature of geomagnetic signal. The multifractal behavior of a signal is generally characterized by the width of multifractal spectrum (h_w) as well as spectrum width h_{wn} correspond to $-q$ to 0 and h_{wp} correspond to $+q$ to 0 also assist in characterizing the specific nature of the geomagnetic signal (Figure 4). Apart from spectrum width parameter, holder exponent parameters, such as h_{min} , h_{max} , $h(0)$, and f_{max} are also useful to characterize the nature of pre-earthquake geomagnetic signal (Figure 4).

3.2.1 Multifractal spectrum width

The width of multifractal spectrum deciphers the nature of complexity of analyzed signal; higher spectrum width indicates larger degree of heterogeneity. A synthetic test of multifractal spectrum on fraction Brownian motion signals (fBm) with Hurst exponents 0.2, 0.4, and 0.5 show increasing width of multifractal spectrum respectively (Figure S3). Moreover, the multifractal spectrum width of combined signal show highest values, indicating increasing nature of complexity, which was not accurately determined by the monofractal dimension. The width of multifractal spectrum (h_w , h_{wp} and h_{wn}) of a sliding window of 1800

data points (half an hour) without overlapping is computed for whole time series of vertical component of 273
 Z-component (Figure 5). The 15-day moving mean of variation in spectrum width of multifractal spectrum 274
 shows significant variations in the range of 0.09 to 0.26. Enhancements greater than threshold value ($\mu +$ 275
 σ) are considered as an anomaly in fractal dimension; . Enhancement in at least one of the components h_w , 276
 h_{wp} and h_{wn} is considered as significant perturbation of the geomagnetic signal (Figure 5). The 277
 enhancements in h_w , h_{wp} and h_{wn} components with corresponding earthquakes is summarized in Table T3. 278
 For the earthquake swarm of 31 Mar-18 Apr, 2019 (moderate magnitude 4.5-5.3, shallow focal depth 15- 279
 30km, and epicentral distance 50-100 km), a preceding enhancement (in h_w , h_{wp} , and h_{wn}) component 280
 occurred during 17-22 Mar, 2019. The significant enhancement during 14 May (in h_w component), 14-15 281
 and 17-20 May, 2019 (in h_{wp} component) and 29Apr-5 May, 2019 (in h_{wn} component) are partly common 282
 to each other and occurred prior, co and post of earthquake 16th and 17th May, 2019 (moderate magnitude 283
 (4.5-4.8), focal depth (10-27.4), and epicentral distance (58-71)). The two sets of enhancement during 22- 284
 25 May, 2019 and 4-22 Jun, 2019 (in h_w and h_{wp}) and one persistence enhancement during 8-22 Jun, 2019 285
 occurred prior to earthquake 19 Jun, 2019 (M 4.6, focal depth 60 km, and epicentral distance 60 km). the 286
 enhancement in common duration 30-9th Jul, 2019 (different duration of persistence) and no enhancement 287
 in h_{wn} component occurred prior to two earthquakes 9th Jul, 2019 at two different locations with moderate 288
 magnitude (4.5), moderate and shallow focal depth (80 and 22 km) and large epicentral distance (185 and 289
 156 km). The common enhancement during 17-19th Jul, 2019 in h_w and h_{wn} component (not same duration 290
 of persistence) occurred prior to earthquake on 21st Aug, 2019 (M 4.8, focal depth 10 km, and large 291
 epicentral distance 219 km). the common enhancements during 9-15 Oct, 2019, 7-10th Nov, 2019, in h_w 292
 and h_{wp} component, 11-12th Nov in h_w , and 2-3, 12-14th Nov, 2019 in h_{wp} component occurred prior to 293
 earthquake 17th and 20th Nov, 2019 with moderate magnitude (4.7-5.1), focal depth (10-25 km), and 294

epicentral distance (60-91 km). Further, the four-earthquake occurred during December, 2019 and 1st week of Jan, 2020 is not (moderate magnitude, moderate focal depth, and moderate to large epicentral distances) preceded by any significant enhancement in components of multifractal width parameter. The common enhancements during 16-20 Jan, 2020 in h_w and h_{wp} component occurred prior to earthquake 22nd (M 4.6, focal depth 100km, and epicentral distance 77) and 28th Jan, 2020 (M 4.9, focal depth 24km, and epicentral distance 204 km). Further, the two-earthquake event of May-2020 (moderate magnitude, shallow focal depth, and large epicentral distance) is not preceded by any enhancement in components of multifractal width parameter.

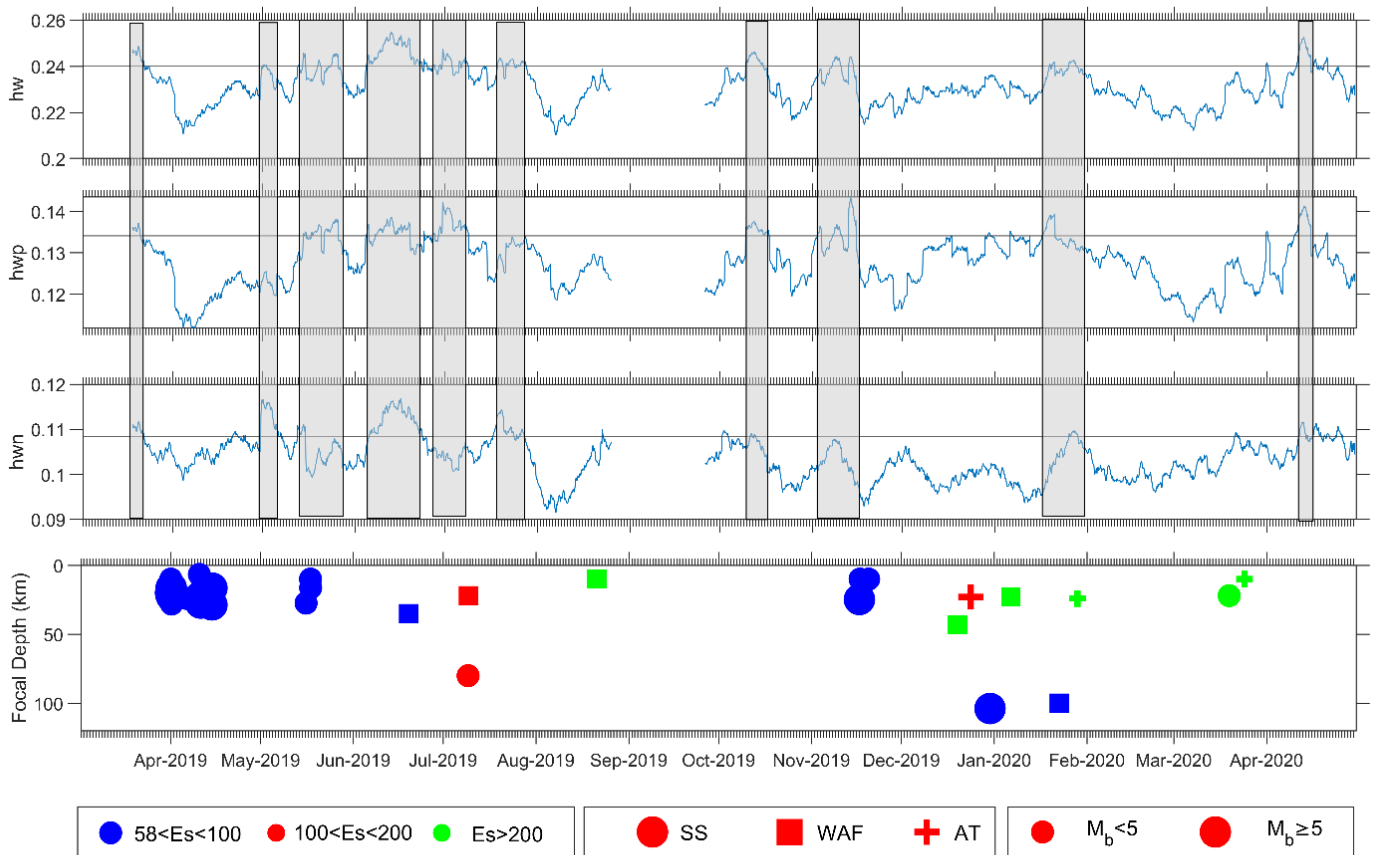


Figure 5. Temporal variation in spectrum width h_w , h_{wp} and h_{wn} from top panel and anomalous behavior are highlighted by grey color. The bottom panel showing the occurrences of earthquake with magnitude (size of circle) and corresponding faults (different color). Top four panel showing the detail view of Jun 2019 month.

3.2.2 Holder Exponent

The holder exponent parameters (h_{max} , h_{min} , $h(0)$, and f_{max}), used for defining the multifractal spectrum curve also show significant variations in the amplitude; again enhancements greater than threshold value (1.0082, 0.4626, 0.5873, 0.3612) are treated as significant (Figure 6). The enhancements in h_{max} , h_{min} , $h(0)$, and f_{max} components with corresponding earthquakes are summarized in Table T4.

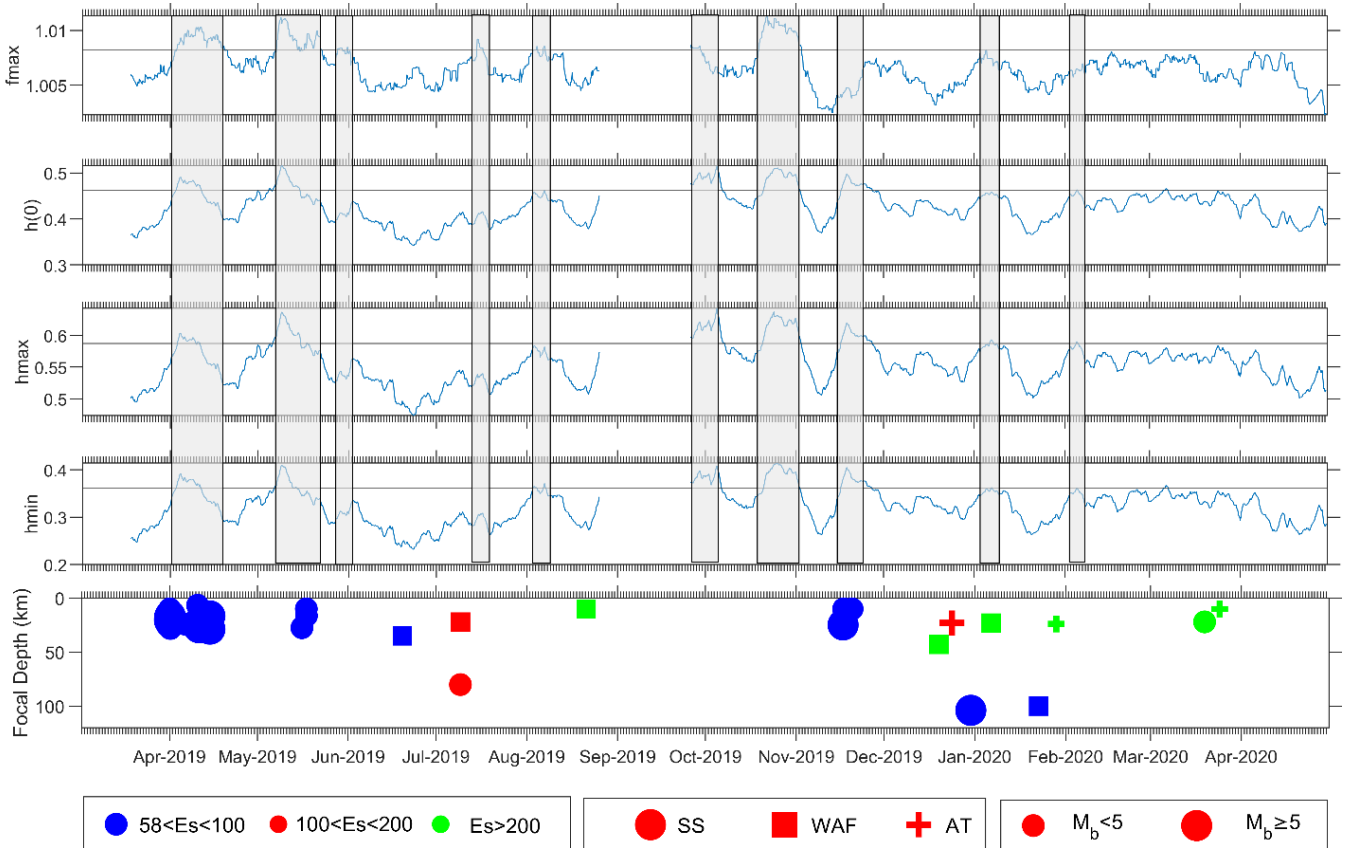


Figure 6. Temporal variation in holder exponent parameters i.e. f_{max} , h_{fmax} , h_{max} and h_{min} from top panel and anomalous behaviour are highlighted by grey colour. The bottom panel showing the occurrences of earthquake with magnitude (size of circle) and corresponding faults with different color.

The common enhancements during 2-18 April, 2019 in all components of holder exponent coincide with the swarm of earthquake 31st 18th April, 2019 with moderate magnitude, moderate focal depth, and moderate to large epicentral distance. The next common enhancements are noted during 6-14 May, 2019 in all components of holder exponent prior to the three earthquakes (moderate magnitude, focal depth and epicentral distance), one 16th May, 2019, and two 17th May, 2019. For the same earthquakes two small co and post seismic enhancements are noted in f_{max} component during 17-19 May, 2019. The small enhancement in only f_{max} during 20-21 May, 2019 is preceded by the earthquake 19th Jun, 2019 with moderate magnitude, focal depth, and epicentral distances. Further, the two-earthquake event of 9th July with moderate magnitude, epicentral distance, large epicentral distance and different location is not preceded by enhancements in any component of holder exponent. Two small enhancements during 15-16 Jul, and 6 Aug, 2019 in f_{max} component and two small enhancements in h_{min} during 6 Aug, 2019 occurred prior to the earthquake 21 Aug, 2019. The two enhancements common in all components but different durations, one small during 26 Sep-5Oct, 2019 and persistence during 16 Oct-24 Nov, 2019 occurred prior as well as coincident and post three earthquakes. Two of them were at similar location 17th Nov, 2019 and one at a different location 20th Nov, 2019 with moderate magnitude, shallow to very shallow earthquake, and moderate epicentral distance. Further, the three-earthquake occurred in December, 2019, the first two with moderate magnitude and focal depth and large epicentral distance and third with moderate magnitude, large focal depth, and moderate epicentral distance are not preceded by enhancement in any component of

holder exponent. The next small enhancement in h_{max} component only during 3-8 Jan, 20020 is coincident with earthquake of 06th Jan, 2020 (mod. Magnitude, mod. Focal depth, and large epicentral distance) and preceded by two earthquakes on 22 and 28th Jan, 2020 (with moderate magnitude, moderate and large focal depth; large and moderate epicentral distance).

For the earthquake swarm of 31 March, 2019 and early April, the spectrum width shows a small enhancement during 17-20th March, that is 12 days prior to the earthquake cluster, which have magnitudes between 4.5 to 5.3 and occur in a small region along the SS fault. There is no enhancement of the Holder exponent. For the intermittent earthquakes in mid-April, there is no signal in the spectrum width but the Holder exponent shows a consistent enhance during 3-10 April, a week before the main cluster. In early May, upto 5th, h_{wn} shows an enhancement; the pattern is mimicked in the Holder exponent without crossing the threshold value. Small anomalous enhancements 12-14th May on the h_{wn} , h_{wp} and h_w of spectrum width, just prior to the moderate earthquakes on 16th and 17th May. The holder exponent exhibits a longer, more consistent enhancement during 7-14th May, f_{max} shows a co-seismic anomaly on 17-19 May, followed by anomalies on 20-21 May. Post seismic perturbations are also noted in the spectrum width. For the M4.6 earthquakes of 19th June, long duration anomalies are seen in spectrum width but not in Holder exponent. For the dual earthquakes on 9th July, pre and post seismic anomalies are seen in spectrum width; only one anomaly is seen in Holder exponent during 14-16 June. There is no significant multifractal anomaly for the 21 Aug, very shallow earthquake. In October 2019, significant repeated anomalies are observed in Holder exponent right till Nov, 2019. In the second half of Jan and much of February, there are several individual earthquakes; no significant enhancement is observed for any of them. A short enhancement can be noted in 11-14 April, which would be indicative of a future event.

3.3 Combined result of monofractal and multifractal analysis

Figures 4, 5, and 6, show that all the components from monofractal and multifractal, have different response 356
for each earthquake, indicating different characteristics of signal, which can be used as indicator of pre- 357
earthquake processes in the focal zone of earthquake. In this regard, we have characterized the 358
enhancements of components in three types of patterns: (i) present in only monofractal component, (ii) 359
present in only multifractal components, and (iii) present in monofractal as well as in multifractal 360
component. The significant enhancement from both parameter (monofractal and multifractal) with 361
corresponding earthquake from figure 4, 5, and 6 is summarized in Figure 7. 362

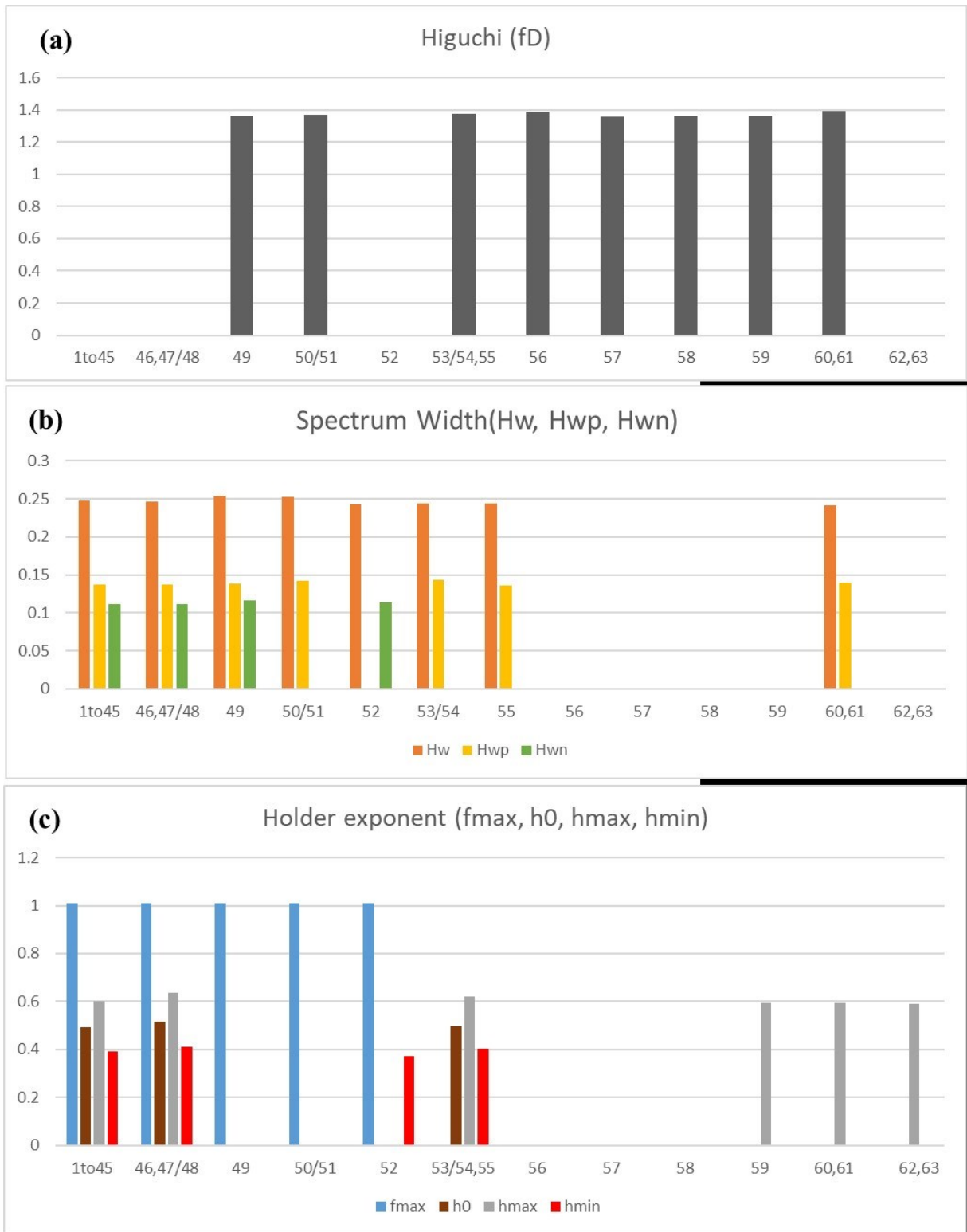


Figure 7. The components of significant enhancement with corresponding earthquakes from (a) Higuchi fractal dimension, (b) Spectrum width, and (c) Holder exponent.

From Figure 7 it is evident that the Higuchi fractal dimension from monofractal analysis exhibits significant enhancements corresponding to earthquake 56, 57, and 58, while there are no enhancements in multifractal

component correspond to same earthquake. Furthermore, there are significant enhancements in multifractal 385
components correspond to the earthquake 1-45 (swarm of earthquake), 46, 47/48, 52, 62, and 63, while 386
there are no enhancements in monofractal component (or Higuchi fractal dimension). It is also noted that 387
the earthquake 1-45, 46, 47/48 exhibit to all component of spectrum width (h_{wn} , h_{wp} and h_w) and holder 388
exponent f_{max} , h_{max} , h_{min} , and $h(0)$, while for earthquake 52 (h_w , h_{wn} , h_{min} , and f_{max}), 62 (h_{max}), and 389
63 (h_{max}) all components of multifractal parameters are not present. Similarly, the significant 390
enhancements correspond to earthquakes 49, 50/51, 53/54, 55, 59, 60, and 61 observed in monofractal as 391
well as multifractal components, but not in all components of multifractal. From multifractal parameters it 392
is also noted that, h_w component of spectrum width is present in each enhancement, h_{max} component is 393
present with each except for the 49, 50/51, and 52 earthquakes. Similarly, enhancements in f_{max} along with 394
spectrum width h_w is present for all the earthquakes except 53/54, 55, 60, 61. Significant enhancements for 395
days where the Kp index is greater than 3 and Dst index smaller than -50 have been identified and removed 396
from the study, although such short duration effects are diminished considerably after averaging of each 397
component with 15 day moving mean (Figure 8). An additional component of diurnal ratio is also appended 398
for correlation with monofractal and multifractal components, which is also treated with criteria of 399
planetary index (figure 8). 400

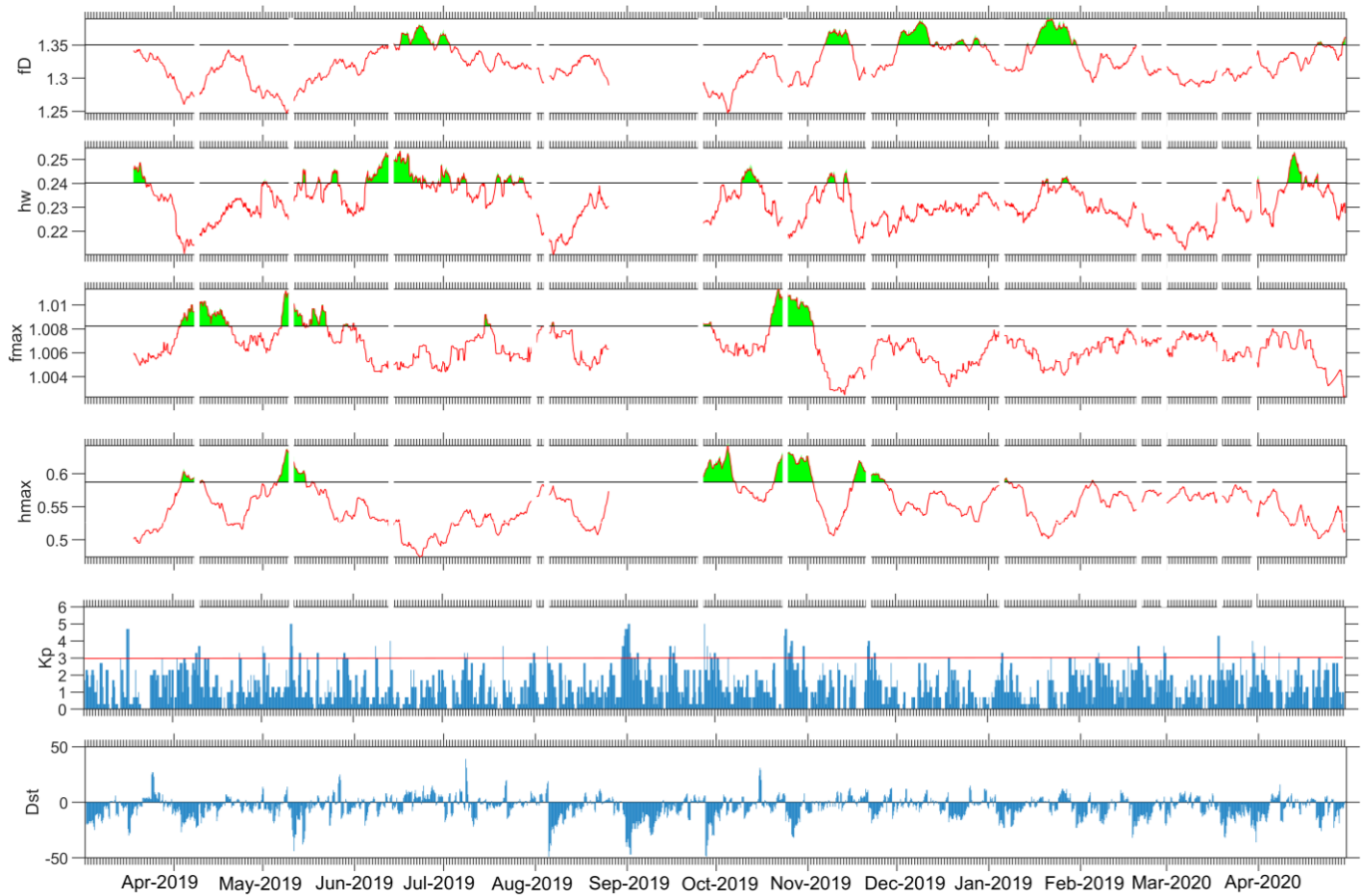


Figure 8. Temporal variation of (a) Higuchi fractal dimension, (b) spectrum width component of multifractal width parameter, (c) f_{max} component, and (d) h_{max} component after removing the data correspond to (f) $K_p > 3$ and (g) $Dst < -50$.

Therefore, from multifractal analysis, h_w , h_{max} , and f_{max} components, and Higuchi fractal dimension from monofractal parameter has traced all the significant signatures corresponding to the seismogenic activity in the earthquake. The month-wise analysis from Mar-2019 to April -2020 of each component preferred for detail analysis of enhancements shown in Figure S4-S17. From the total duration of analysis, we have selected two quiet days 25th May and 3rd Aug – 2019 and shown the geomagnetic field variation on corresponding date (figure S18), in which first is showing quite disturbed signatures (also showing high multifractal values) compare to second (showing smaller multifractal values). This suggests that the

disturbance in geomagnetic field on the quiet day 25th May, 2019 is highly possible due to interference of EM fields.

Discussion:

We examine the combined observations of signatures from monofractal or Higuchi fractal dimension (f_D) and multifractal components (h_w , h_{max} and f_{max}) along with diurnal ratio to unravel a linked pattern, which can be interpreted as related to earthquake processes (Figure 9). A swarm of earthquakes (1-45 as per our catalogue) along the SS fault occurred around the first week of April 2019. The data is available from 15th March and no anomalies were identified in the Diurnal ratio; hence it was concluded that data length was insufficient (Prajapati and Arora, 2024). While no anomalies were detected in the f_D , distinct enhancements are noted in the Spectrum width 14 days prior to the beginning of the swarm. Co-seismic f_{max} over the entire duration and muted h_{max} enhancements are noted during 2-18 April and 2-10 April respectively.

For the moderate magnitude, shallow focus earthquakes 46, 47, 48, clustered close together during mid-June 2019, Diurnal ratio shows a significant enhancement 50 days before the events, whereas no anomalies are recorded in f_D . Enhancements in both h_{max} and f_{max} start 11 and 9 days before the events and continue co-seismically.

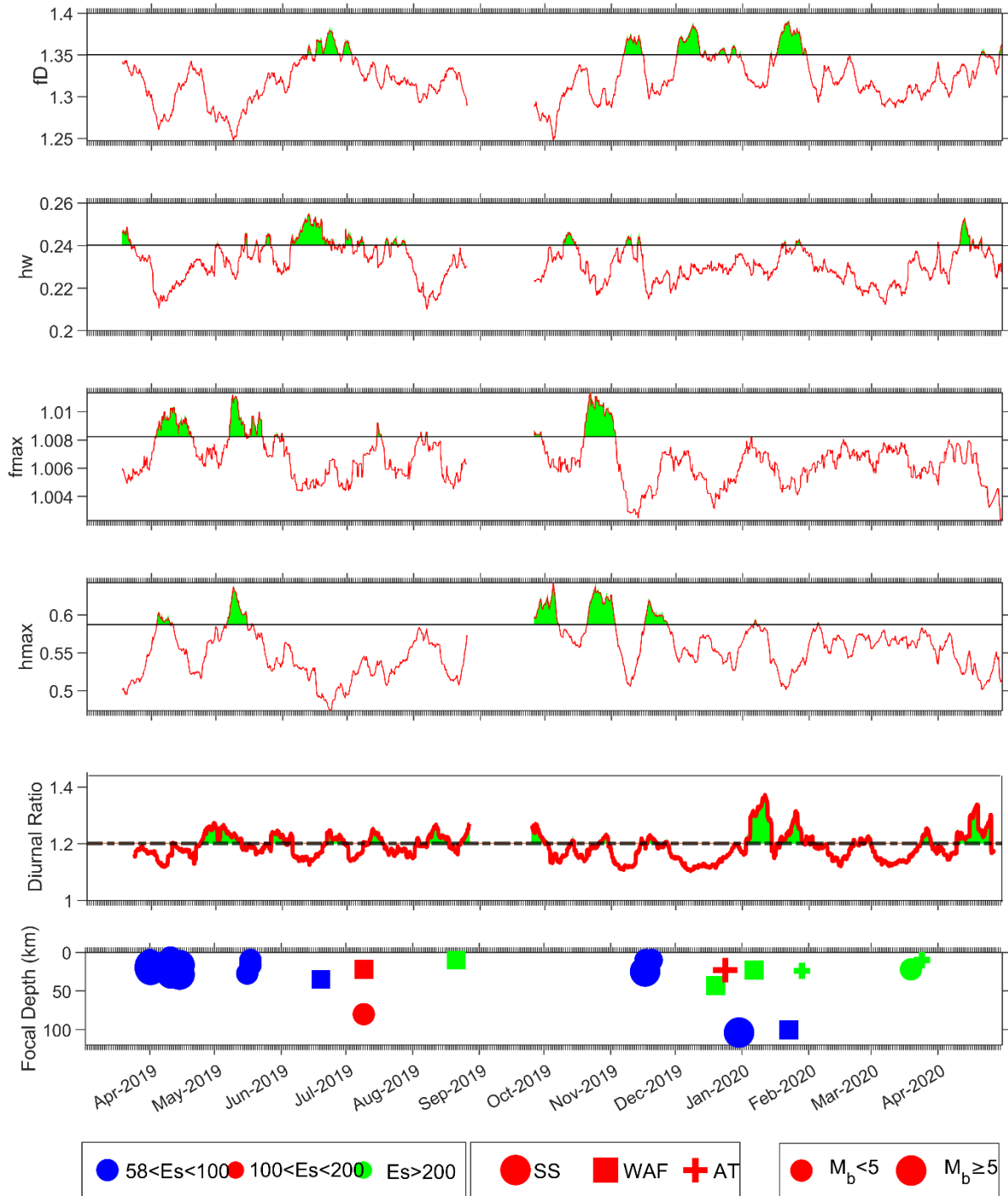


Figure 9. The significant enhancement in temporal variation of (a) Higuchi fractal dimension, (b) spectrum width component of multifractal width parameter, (c) fmax component showing the holder exponent presence highest number of time (d) hmax component showing the largest value of holder exponent, and (e) diurnal ratio, indicated by shaded green color, (f) the occurrences of earthquakes in same time duration with magnitude and focal depth.

453
454
455
456
457

Earthquake 49 on 19th June 2019 was of moderate magnitude, moderate focal depth and moderate epicentral distance on the WAF. It is preceded by small enhancement in Diurnal ratio 22 days before, f_D 7 days prior and continues co-seismically. Spectrum width enhancement starts 15 days prior to event, which continues co-seismically, there are no signatures in h_{max} or f_{max} .

The dual earthquakes 50 and 51, occurred soon after 49, at large epicentral distances on the WAF (shallow focal depth) and on the SS (deep focal depth) in opposite directions to the recording station. Diurnal ratio shows a significant anomaly 16 days prior to the event, accompanied by slight increase in f_D 19 days before. Mild perturbations are also observed in Spectrum width 9-4 days before the events.

The earthquake 52 is similar to 49, with shallower focal depth and very large epicentral distance of 219 km on the WAF. It is preceded by enhancement in Diurnal ratio is seen 14 days before, no signatures are seen in any other parameter.

The earthquakes 53, 54, 55 on 17 and 20 Nov 2019, occur along the SS fault with moderate epicentral distances and shallow focal depth; 53 has magnitude of 5. They are preceded by two phases of small enhancements in Diurnal ratio 21 and 3 days before the earthquakes, continuing to co-seismic signatures. Enhancements in h_{max} continue to co-seismic signatures. Signatures in h_w are very muted, f_D shows significant enhancement 2 days prior to the earthquakes.

Earthquakes 56-63 are individual events, from end of 2019 to first quarter of 2020, separated by several days to weeks intervals in between. Earthquake 56 has very large epicentral distance, also occurring on the WAF like earthquake 52, but with a focal depth of 43 km. This is followed by 57, which is a M=5 earthquake at very shallow focal depth, at large epicentral distance on the AT. 58 occurred on Dec 30, 2019, an M=5 event on the SS fault with large focal depth and moderate epicentral distance. The events are preceded by a significant enhancement in f_D , but no other signatures. With only one station, it is not possible to construct an

earthquake-anomaly link for this scenario. The cluster of 53-54-55, for which signatures are noted in Diurnal 480
ratio, f_D , and h_{max} , occurred in a closer duration period, on the same SS fault at moderate epicentral distances 481
and are also at shallow focal depth. The earthquake 59 is of moderate magnitude, shallow focal depth but large 482
epicentral distance on the WAF. Curiously, a co- and post seismic enhancement in diurnal ratio is the sole 483
signature for this event. For the earthquakes 60 (large focal depth and moderate epicentral distance on the 484
WAF) and 61 (shallow focal depth and large epicentral distance on the AT), co-seismic enhancement in 485
diurnal ratio is accompanied by similar enhancement in f_D . Earthquakes 62 (moderate magnitude, shallow 486
focal depth and large epicentral distance on the AT) and 63 (moderate magnitude, shallow focal depth and 487
large epicentral distance also on the AT), no preceding signatures are observed on any of the parameters. 488
However, a distinct post seismic increase in diurnal ratio is noted. 489

In April 2020, enhancements in h_w during 10-14 April and Diurnal ratio during 10-24 April are observed. 490
Several research articles are available (Hayakawa et al., 1999; Gotoh et al., 2003; Ida et al., 2012) to study the 491
behavior of geomagnetic signal using non-linear signal processing techniques such as monofractal and 492
multifractal in context of EM field generated from local sources due to seismogenic activity. Hayakawa et al. 493
(1999) have analysis on H, D, and Z component of ULF geomagnetic signal recorded at 65 km from the 494
epicenter of Guam earthquake with M8 occurred on 8th Oct, 1993 at focal depth of around 60 km carried using 495
fractal (spectral method) and Hurst exponent analysis (rescaled scaled range R/S method). They inferred that 496
decreasing value of slope (β) from 2.5 to ~ 1 before the earthquake, which can be considered as an indicator 497
of SOC, where $\beta \sim 1.1$ is critical value prior to the earthquake. However, no significant changes observed in 498
Hurst exponent by R/S analysis. The large-scale variation and decrease in ULF spectrum slope (or increase in 499
fractal dimension) means increase high frequency fluctuations is a proxy measure of small-scale fractal 500
structure cause by active microfracturing process followed by generation of seismogenic ULF emission. In 501

our study, we have also noticed the increase in fractal dimension atleast 10 days prior to the earthquake (49,50- 502
51,53-55, and 60-61) with moderate magnitude ($4.5 < M < 5.1$), shallow and moderate focal depth (35, 51,14, 503
and 62km), as well as small, moderate, and large epicentral distance (60, 170, 76, and 140km). The increasing 504
fractal dimension before the earthquakes are suggests the microfracturing process in Earth's crust to be the 505
cause of generation and emission of EM field in the vicinity of recording station. 506

Gotoh et al. (2003) have analyzed the ULF geomagnetic data recorded at three stations on Izu peninsula, 507
Japan, where a nearby strong earthquake swarm started from 26, June to August 2000 with magnitude upto 508
6.5. An eruption of volcanic also started simultaneously in Miyakejima Island. Izu region on Philippine plate 509
is under tensile stress and seismically very active because of subduction of Pacific plate at Nankai and Sagami 510
Troughs (Uyeda et al., 2002). The monofractal dimension of the H component shows an increase a week 511
before the earthquake. In present study, we have analyzed Z-component instead of H-component, because 512
recent studies suggested that Z-component is more sensitive for EM fields generated from local sources. In 513
our study we did not find any significant signature of enhanced fractal dimension of Z component one week 514
prior to a swarm of 45 earthquakes from 31-Mar to 18-April, 2019, however an enhancement in spectrum 515
width parameter (h_w), 10 days before the swarm activity started. 516

Further, (Ida et al., 2005) carried out the multifractal analysis on H component of geomagnetic signal recorded 517
at 65 km from the epicenter of Guam earthquake occurred on 8th Oct, 1993 at focal depth of around 60 km. A 518
westward movement of the Pacific plate and its subduction under Philippine plate triggered the Guam 519
earthquake (Ms 8.0) at shallow dipping subduction zone with a strike slip fault along the trench (Harris, 1993). 520
Ida et al. (2005) found significant changes in the multifractal parameters of Holder exponent and spectrum 521
width (α_{min} , α_{max} , w , Δ , f_{max} , $\alpha(f_{max})$, and D_q , for $q < 0$, $q > 0$, and $q = 0$). The observation of 9 days 522
running mean of spectrum width w and α_{max} shows clear and significant variation 30 days prior to the 523

earthquake. In our analysis of multifractal parameters from moderate subduction zone earthquakes, with focal 524
depth in range of 10-30 km, the 15-day running mean of Spectrum width and Holder exponent show significant 525
enhancements 12 and 20 days prior to those earthquakes, which occurred close in time as a cluster (1-45, 47- 526
48, 50-51, 53-55). This difference in pattern may be due to the large differences in magnitude of the studied 527
earthquakes. 528

Ida et al. (2012) analyzed the fractal dimension (estimated by Higuchi method) of ULF data recorded at Kashi 529
station, China, approximately for four years (Mar, 2003 to Dec, 2006), in which several moderate earthquakes 530
occurred (greater than 5.0 and close to 6) at epicentral distances of 100 to 125, including one earthquake at 531
approximately 300 km. The region is seismically very active due to relative movement of plates along SAF 532
fault (normal fault) is locally dominant in the area (He et al., 2015). Ida et al. (2012) applied the criterion of 533
 $\mu \pm 2\sigma$ to define the significant variations of the fractal dimension and reported decrease in the Z component 534
for two earthquakes (M 5.7 and M 5.4) while earthquakes with magnitude greater than 5 did not show any 535
signature. The enhancement in f_D is interpreted as indication of dominance of high frequency component and 536
decrease in f_D as dominance of low frequency component, which may correlate with the high frequency 537
mechanism like micro-fracturing and slow processes like electrokinetic effect respectively. Potirakis et al. 538
(2017) has analyzed geomagnetic data (H, D, and Z) at station Kakioka (KAK) at epicentral distance of 300 539
km from Tohoku earthquake (M 9.0) of 11 March, 2011. The earthquake was caused by the rupture of a stretch 540
of the subduction zone associated with the Japan Trench, which separates the Eurasian Plate from the 541
subducting Pacific Plate. The data analyzed using DFA and Higuchi method, observed a significant decrease 542
in spectral exponent (using DFA) and corresponding increase in fractal dimension (using Higuchi method) 5- 543
6 months prior to the large magnitude Tohoku earthquake. In our study, we have found significant 544
enhancements with the criterion of $\mu + \sigma$, producing pre-seismic increases in f_D for multiple earthquake 545

occurrences (50-51, 53-55) with $4.6 < M = 5$ and either shallow focal depth or small epicentral distance, 19 and 11 days before the earthquakes.

In our work, we have applied both mono and multifractal analysis to the geomagnetic Z component data, the differences in the trends of the fractal parameters reveal interesting inferences (Table 1). We have defined four clusters of the earthquakes under study (1-45, 47-48, 50-51, 53-55). There are 10 earthquakes, which occurred as single events. For the single events 52, 56-63 ($4.5 < M < 5.0$), which are characterized by either large focal depth (>100 km) or large epicentral distance (~ 200 km), signatures in multifractal parameters. We infer that the EM fields from such moderate magnitude and large epicentral distance earthquakes are too weak to detect by multifractal and diurnal ratio approach (Prajapati and Arora., under review). For the same single events (with focal depth >100 km or epicentral distance ~ 200 km), we observed that enhancements in f_D corresponding to earthquakes 56, 57, 58, 60, and 61 while the earthquake 52, 59, 62, 63 are not correspond to any pre-co or post enhancements in f_D parameter. The significant enhancement corresponds to 5 events out of 9, including two co-seismic signature (60 and 61) indicate the greater efficacy of f_D parameter than multifractal parameter for single events with focal depth >100 km or epicentral distance ~ 200 km. The earthquake 52 is associated with an increase in the Diurnal ratio 13 days in advance. The single event 49 is characterized by moderate focal depth and epicentral distance, which is associated with co-seismic enhancements in f_D , pre-seismic signatures in h_w (7 days prior) and diurnal ratio (15 days prior).

The clusters, on the other hand, produce prominent signatures in the multifractal parameters. The first cluster (1-45) has signature in h_w (14 days prior) and a co-seismic enhancement in f_{max} . The second cluster (47-48) has signatures in f_{max} , h_{max} and diurnal ratio, 9, 9, 13 days prior to event respectively. The third cluster (50-51) at a larger epicentral distance of 165 km, has signatures in f_D , h_w and diurnal ratio 19, 9, 19 days prior to event respectively. The fourth cluster (53-55) includes earthquakes of $M=5.1$ and the events are at shallow

focal depth and small-to-moderate epicentral distances produce signatures in f_D and all the multifractal parameters as well as diurnal ratio.

The combined observation from fractal (mono and multifractal) and diurnal ratio (Table 1) clearly indicates that the fractal parameters exhibit significant enhancement associated with 10 earthquakes (including co-seismic signatures), while significant enhancements in diurnal ratio are correlated with nine earthquakes out of ten (including two post-seismic signatures).

Table 1: The following table summarizes the earthquake and its characteristics presence (Y) or absence (-) of potential enhancements in monofractal (f_D) and multifractal (h_w, f_{max}, h_{max}) components and diurnal ratio.

EQ. No.	Magnitude	Focal Depth (Km)	Epicentral Distance (Km)	Single /Cluster (S) (C)	f_D	h_w	f_{max}	h_{max}	Diurnal ratio
1-45	-	Moderate	Moderate	C	-	Y	Co-	-	-
46-48	Moderate	Moderate	Moderate	C	-	-	Y	Y	Y
49	Moderate	Moderate	Moderate	S	Co-	Y	-	-	Y
50-51	Moderate	Shallow/ Large	Large	C	Y	Y	-	-	Post-
52	Moderate	Shallow	Large	S	-	-	-	-	Y
53-54-									
55	Large	Shallow	Small	C	Y	Y	Y	Y	Y
56	Moderate	Moderate	Large	S	Y	-	-	-	-
57	Large	Shallow	Large	S	Y	-	-	-	-
58	Large	Large	Mod	S	Y	-	-	-	-
59	Moderate	Shallow	Large	S	-	-	-	-	Y
60	Moderate	Large	Moderate	S	Co-	-	-	-	Y
61	Moderate	Shallow	Large	S	Co-	-	-	-	Y
62	Moderate	Shallow	Large	S	-	-	-	-	-
63	Moderate	Shallow	Large	S	-	-	-	-	post

According to Ida et al. (2012), significant enhancements in fractal values of geomagnetic signal recorded in tectonic active areas are representing the dominance of high frequency component associated with EM field from microfracturing processes in lithosphere. Apart from this, the components of holder exponent (part of multifractal analysis) such as f_{max} , h_{max} , h_{min} , and $h(0)$ also analyses the different characteristics of the signal (Krzyszczak et al., 2019) such as enhancement in h_{max} indicates that underlying process of events are more smooth rather than sorter fluctuations while h_{min} is just opposite to h_{max} . Similarly, f_{max} is correspond to $h(0)$ i.e. h which occurred maximum number of times in range $h_{max} - h_{min}$. The enhancements in f_{max} value with large h indicate the underlying processes is less correlated and fine structure i.e. signal embedded with anomalies and not completely regular while f_{max} correspond to smaller value of h indicate the highly correlated and most regular signal. Enhancements in h_{max} and f_{max} with $h(0)$ correspond to large h of a geomagnetic signal recorded in active tectonic area, indicates that the underlying processes is smooth and exhibit anomalies (less correlated and fine structures) of low frequencies. According to Conti et al. (2021) electrokinetic process is responsible for generation of low frequency EM signature from lithospheric deformation of a focal zone.

The enhancements in h_{max} and f_{max} , preceding the clusters of shallow earthquakes 1-45, 46-48, 53-55 on the SS fault at moderate epicentral distances are indicative of low frequency perturbations from multiple sources, which are ascribed to electrokinetic processes (Conti et al., 2021). For the cluster 50-51, the former occurs on the SS fault and the latter on the WAF leading to interferences of the EM signals, whereby the h_{max} and f_{max} enhancements are not prominent.

The earthquakes 49, 51 and 52 on the WAF dominated by strike slip mechanisms are also shallow and are at moderate epicentral distances but have enhancements in f_D and h_w , the latter being more significant. This is interpreted as high frequency perturbations attributed to microfracturing processes (Ida et al., 2012).

The earthquakes 56, 57, 59, 60, 61, 63 on the WAF and AT faults at large epicentral distances are linked with enhancements in f_D and h_w , the former being more significant. We interpret these high frequency perturbations to be also generated due to microfracturing processes; the large epicentral distances possibly leading to attenuation of the highest frequency components leads to more prominent monofractal signatures. The earthquakes 50, 58 and 62 are either at very large epicentral distances or large focal depths and fail to produce signatures in any of the fractal components.

Thus, the moderate focal depth and epicenter distance earthquakes on WAF are dominated by h_w while large focal depth and epicentre distance earthquakes on WAF/AT dominated by f_D possibly indicating that the EM field from large distance are more homogeneous due to attenuation and dominating its appearance in f_D component, while EM field from short distance, indicating that EM field are more heterogeneous and dominating its appearance in h_w component. Which means, f_D component is most sensitive component for large epicentre and focal depth earthquakes while h_w component is more sensitive for moderate epicentre distance and focal depth earthquakes.

5. Conclusions

The study of fractal natures of the geomagnetic time series (Z component) allows us to conclude:

- (i) The earthquake clusters occurred on normal/thrust fault are of moderate magnitude and focal depth are emitting prior EM fields of low frequency effectively generated from electrokinetic processes in focal zone of earthquake.
- (ii) The single earthquakes occurred on strike slip WAF fault of moderate magnitude and focal depth are emitting prior EM field of more heterogeneity and frequency while, earthquakes on same fault with large epicentre distance/ focal depth emitting prior EM field of lesser heterogeneity and high frequency effectively generated from microfracturing processes in focal zone of earthquake.

- (iii) The monofractal dimension f_D is more effective to trace the EM field from large epicentre distance and focal depth while multifractal spectrum width h_w is more effective to trace the EM field from moderate to small epicentre distance and focal depth for the case of microfracturing processes.
- (iv) The fractal analysis has advantage over diurnal ratio is simultaneous observation of high and low frequency EM field from lithospheric deformation of focal zone of earthquake, which are emitted from different pre-earthquake processes.

Statements and Declarations

(i) Data Availability

The data that support the findings of this study are available upon reasonable request.

(ii) Competing Interests

The authors have no relevant financial or non-financial interests to disclose.

(iii) CRediT authorship contribution statement

All authors contributed to the study conception and design. Methodology and data collection were performed by Kusumita Arora, and Rahul Prajapati. Data curation and its analysis using MATLAB coding was performed by Rahul Prajapati. The first draft of the manuscript was written by Rahul Prajapati. Review and editing of first draft of the manuscript performed by Kusumita Arora, and the work carried out under supervision and validation of Kusumita Arora. All authors read and approved the final manuscript.

Acknowledgments: The Authors are thankful to the Director CSIR-National Geophysical Research Institute, India for granting permission to access the data for research purpose and to publish the work (Ref. No. NGRI/Lib/2024/Pub-019). The authors acknowledge the available public domain data sets from WDC Kyoto (<https://wdc.kugi.kyoto-u.ac.jp/>) and earthquake data from ISC catalogue (<http://www.isc.ac.uk/iscbulletin/search/catalogue/>). Authors are also acknowledging the Dr. N. Phani

Chandrasekhar and other observatories staff for maintaining the remote site observatories to acquire the
uninterrupted data.

References

- Bak, P., Tang, C., and Wiesenfeld, K.: Self-organized criticality, *Phys. Rev. A*, 38, 364, 1988.
- Barabási, A.-L. and Vicsek, T.: Multifractality of self-affine fractals, *Phys. Rev. A*, 44, 2730, 1991.
- Bella, J., Brodsky, B., and Berman, H. M.: Hydration structure of a collagen peptide, *Structure*, 3, 893–906, 1995.
- Bhattacharya, K. and Manna, S. S.: Self-organized critical models of earthquakes, *Phys. A Stat. Mech. its Appl.*, 384, 15–20, 2007.
- Bulusu, J., Arora, K., Singh, S., and Edara, A.: Simultaneous electric, magnetic and ULF anomalies associated with moderate earthquakes in Kumaun Himalaya, *Nat. Hazards*, 1–31, 2023.
- Borovsky, J. E. and Valdivia, J. A.: The Earth’s magnetosphere: a systems science overview and assessment, *Surv. Geophys.*, 39, 817–859, 2018.
- Chadha, R. K., Singh, C., and Shekar, M.: Transient changes in well-water level in bore wells in Western India due to the 2004 M W 9.3 Sumatra Earthquake, *Bull. Seismol. Soc. Am.*, 98, 2553–2558, 2008.
- Conti, L., Picozza, P., and Sotgiu, A.: A critical review of ground based observations of earthquake precursors, *Front. Earth Sci.*, 9, 676766, 2021.
- Crampin, S., McGonigle, R., and Bamford, D.: Estimating crack parameters from observations of P-wave velocity anisotropy, *Geophysics*, 45, 345–360, 1980.
- Currenti, G., Del Negro, C., Lapenna, V., and Telesca, L.: Multifractality in local geomagnetic field at Etna volcano, Sicily (southern Italy), *Nat. Hazards Earth Syst. Sci.*, 5, 555–559, 2005.
- Dimri, V. P.: *Fractal behaviour of the earth system*, Springer, 2005.
- Fraser-Smith, A. C., Bernardi, A., McGill, P. R., Ladd, M., Helliwell, R. A., and Villard Jr, O. G.: Low-frequency magnetic field measurements near the epicenter of the Ms 7.1 Loma Prieta earthquake, *Geophys. Res. Lett.*, 17, 1465–1468, 1990.
- Freund, F. and Sornette, D.: Electro-magnetic earthquake bursts and critical rupture of peroxy bond networks in rocks, *Tectonophysics*, 431, 33–47, 2007.
- Gahalaut, V. K., Kundu, B., Laishram, S. S., Catherine, J., Kumar, A., Singh, M. D., Tiwari, R. P., Chadha, R. K., Samanta, S. K., and Ambikapathy, A.: Aseismic plate boundary in the Indo-Burmese wedge, northwest

- Sunda Arc, *Geology*, 41, 235–238, 2013. 679
- Gao, X.-Y., Guo, Y.-J., and Shan, W.-R.: Optical waves/modes in a multicomponent inhomogeneous optical fiber via a three-coupled variable-coefficient nonlinear Schrödinger system, *Appl. Math. Lett.*, 120, 107161, 2021. 680
681
682
683
- Gotoh, K., Akinaga, Y., Hayakawa, M., and Hattori, K.: Principal component analysis of ULF geomagnetic data for Izu islands earthquakes in July 2000, *J. Atmos. Electr.*, 22, 1–12, 2002. 684
685
- Gotoh, K., Hayakawa, M., and Smirnova, N.: Fractal analysis of the ULF geomagnetic data obtained at Izu Peninsula, Japan in relation to the nearby earthquake swarm of, *Natural Hazards and Earth System Sciences*, 229–236 pp., 2003. 686
687
688
- Gotoh, K., Hayakawa, M., Smirnova, N. A., and Hattori, K.: Fractal analysis of seismogenic ULF emissions, *Phys. Chem. Earth, Parts A/B/C*, 29, 419–424, 2004. 689
690
691
- Han, P., Hattori, K., Xu, G., Ashida, R., Chen, C.-H., Febriani, F., and Yamaguchi, H.: Further investigations of geomagnetic diurnal variations associated with the 2011 off the Pacific coast of Tohoku earthquake (Mw 9.0), *J. Asian Earth Sci.*, 114, 321–326, 2015. 692
693
694
- Han, P., Hattori, K., Huang, Q., Hirooka, S., and Yoshino, C.: Spatiotemporal characteristics of the geomagnetic diurnal variation anomalies prior to the 2011 Tohoku earthquake (Mw 9.0) and the possible coupling of multiple pre-earthquake phenomena, *J. Asian Earth Sci.*, 129, 13–21, 2016. 695
696
697
- Harris, S. K.: NATIONAL CENTER FOR EARTHQUAKE The Island of Guam Earthquake of, 1993. 698
- Hattori, K., Serita, A., Gotoh, K., Yoshino, C., Harada, M., Isezaki, N., and Hayakawa, M.: ULF geomagnetic anomaly associated with 2000 Izu islands earthquake swarm, Japan, *Phys. Chem. Earth, Parts A/B/C*, 29, 425–435, 2004a. 699
700
701
- Hattori, K., Takahashi, I., Yoshino, C., Isezaki, N., Iwasaki, H., Harada, M., Kawabata, K., Kopytenko, E., Kopytenko, Y., Maltsev, P., Korepanov, V., Molchanov, O., Hayakawa, M., Noda, Y., Nagao, T., and Uyeda, S.: ULF geomagnetic field measurements in Japan and some recent results associated with Iwateken Nairiku Hokubu earthquake in 1998, *Phys. Chem. Earth*, 29, 481–494, <https://doi.org/10.1016/j.pce.2003.09.019>, 2004b. 702
703
704
705
706
- Hattori, K., Han, P., Yoshino, C., Febriani, F., Yamaguchi, H., and Chen, C. H.: Investigation of ULF Seismo-Magnetic Phenomena in Kanto, Japan During 2000-2010: Case Studies and Statistical Studies, <https://doi.org/10.1007/s10712-012-9215-x>, 1 May 2013a. 707
708
709
- Hattori, K., Han, P., Yoshino, C., Febriani, F., Yamaguchi, H., and Chen, C.-H.: Investigation of ULF seismo-magnetic phenomena in Kanto, Japan during 2000–2010: case studies and statistical studies, *Surv. Geophys.*, 34, 293–316, 2013b. 710
711
712

- Hayakawa, M. and Molchanov, O. A.: Summary report of NASDA's earthquake remote sensing frontier project, *Phys. Chem. Earth, Parts A/B/C*, 29, 617–625, 2004. 713
714
- Hayakawa, M., Kawate, R., Molchanov, O. A., and Yumoto, K.: Results of ultra-low-frequency magnetic field measurements during the Guam earthquake of 8 August 1993, *Geophys. Res. Lett.*, 23, 241–244, 1996. 715
716
- Hayakawa, M., Ito, T., and Smirnova, N.: Fractal analysis of ULF geomagnetic data associated with the Guam earthquake on August 8, 1993, *Geophys. Res. Lett.*, 26, 2797–2800, <https://doi.org/10.1029/1999GL005367>, 1999. 717
718
719
- Hayakawa, M., Itoh, T., Hattori, K., and Yumoto, K.: ULF electromagnetic precursors for an earthquake at Biak, Indonesia on February 17, 1996, *Geophys. Res. Lett.*, 27, 1531–1534, 2000. 720
721
- Hayakawa, M., Ida, Y. U. I., and Gotoh, K.: Multifractal analysis for the ULF geomagnetic data during the Guam earthquake, in: *IEEE 6th International Symposium on Electromagnetic Compatibility and Electromagnetic Ecology*, 2005, Proceedings, 239–243, <https://doi.org/10.1109/EMCECO.2005.1513113>, 2005. 722
723
724
725
- Hayakawa, M., Hattori, K., and Ohta, K.: Monitoring of ULF (ultra-low-frequency) Geomagnetic Variations Associated with Earthquakes, *Sensors*, 7, 1108–1122, 2007. 726
727
- He, P., Wen, Y., Xu, C., Liu, Y., and Fok, H. S.: New Evidence for Active Tectonics at the Boundary of the Kashi Depression , China , from Time Series InSAR Observations *Tectonophysics* New evidence for active tectonics at the boundary of the Kashi Depression , China , from time series InSAR observations, *Tectonophysics*, 653, 140–148, <https://doi.org/10.1016/j.tecto.2015.04.011>, 2015. 728
729
730
731
- Heavlin, W. D., Kappler, K., Yang, L., Fan, M., Hickey, J., Lemon, J., MacLean, L., Bleier, T., Riley, P., and Schneider, D.: Case-Control Study on a Decade of Ground-Based Magnetometers in California Reveals Modest Signal 24–72 hr Prior to Earthquakes, *J. Geophys. Res. Solid Earth*, 127, <https://doi.org/10.1029/2022JB024109>, 2022. 732
733
734
735
- Higuchi, T.: Approach to an irregular time series on the basis of the fractal theory, *Phys. D Nonlinear Phenom.*, 31, 277–283, 1988. 736
737
- Ida, Y., Hayakawa, M., Adalev, A., and Gotoh, K.: Multifractal analysis for the ULF geomagnetic data during the 1993 Guam earthquake, *Nonlinear Process. Geophys.*, 12, 157–162, <https://doi.org/10.5194/npg-12-157-2005>, 2005. 738
739
740
- Ida, Y., Yang, D., Li, Q., Sun, H., and Hayakawa, M.: Detection of ULF electromagnetic emissions as a precursor to an earthquake in China with an improved polarization analysis, *Hazards Earth Syst. Sci.*, 775–777 pp., 2008. 741
742
743
- Ida, Y., Yang, D., Li, Q., Sun, H., and Hayakawa, M.: Fractal analysis of ULF electromagnetic emissions in possible association with earthquakes in China, *Nonlinear Process. Geophys.*, 19, 577–583, <https://doi.org/10.5194/npg-19-577-2012>, 2012. 744
745
746
- Jaffard, S., Lashermes, B., and Abry, P.: Wavelet leaders in multifractal analysis, *Wavelet Anal. Appl.*, 1, 747

219–264, 2006. 748

Johnston, M. J. S., Mueller, R. J., Ware, R. H., and Davis, P. M.: Precision of geomagnetic field measurements in a tectonically active region, *J. Geomagn. Geoelectr.*, 36, 83–95, 1984. 749 750

Kantelhardt, J. W., Zschiegner, S. A., Koscielny-Bunde, E., Havlin, S., Bunde, A., and Stanley, H. E.: Multifractal detrended fluctuation analysis of nonstationary time series, *Phys. A Stat. Mech. its Appl.*, 316, 87–114, 2002. 751 752 753 754

Koizumi, N., Kitagawa, Y., Matsumoto, N., Takahashi, M., Sato, T., Kamigaichi, O., and Nakamura, K.: Preseismic groundwater level changes induced by crustal deformations related to earthquake swarms off the east coast of Izu Peninsula, Japan, *Geophys. Res. Lett.*, 31, 2004. 755 756 757

Kopytenko, Y. A., Matiashvili, T. G., Voronov, P. M., Kopytenko, E. A., and Molchanov, O. A.: Detection of ultra-low-frequency emissions connected with the Spitak earthquake and its aftershock activity, based on geomagnetic pulsations data at Dusheti and Vardzia observatories, *Phys. Earth Planet. Inter.*, 77, 85–95, 1993. 758 759 760

Krzyszczak, J., Baranowski, P., Zubik, M., Kazandjiev, V., Georgieva, V., Cezary, S., Siwek, K., Kozyra, J., and Nieróbca, A.: Multifractal characterization and comparison of meteorological time series from two climatic zones, 1811–1824, 2019. 761 762 763

Liu, J. Y., Tsai, Y. B., Chen, S. W., Lee, C. P., Chen, Y. C., Yen, H. Y., Chang, W. Y., and Liu, C.: Giant ionospheric disturbances excited by the M9.3 Sumatra earthquake of 26 December 2004, *Geophys. Res. Lett.*, 33, 2006. 764 765 766

Mandelbrot, B. B. and Van Ness, J. W.: Fractional Brownian motions, fractional noises and applications, *SIAM Rev.*, 10, 422–437, 1968. 767 768

Meng, J., Wang, C., Zhao, X., Coe, R., Li, Y., and Finn, D.: India-Asia collision was at 24 N and 50 Ma: palaeomagnetic proof from southernmost Asia, *Sci. Rep.*, 2, 925, 2012. 769 770

Molchan, G. and Kronrod, T.: The fractal description of seismicity, *Geophys. J. Int.*, 179, 1787–1799, <https://doi.org/10.1111/j.1365-246X.2009.04380.x>, 2009. 771 772

Molchanov, O. A. and Hayakawa, M.: Generation of ULF electromagnetic emissions by microfracturing, *Geophys. Res. Lett.*, 22, 3091–3094, <https://doi.org/10.1029/95GL00781>, 1995. 773 774

Molchanov, O. A., Kopytenko, Y. A., Voronov, P. M., Kopytenko, E. A., Matiashvili, T. G., Fraser-Smith, A. C., and Bernardi, A.: Results of ULF magnetic field measurements near the epicenters of the Spitak (Ms= 6.9) and Loma Prieta (Ms= 7.1) earthquakes: Comparative analysis, *Geophys. Res. Lett.*, 19, 1495–1498, 1992. 775 776 777

Muzy, J.-F., Bacry, E., and Arneodo, A.: The multifractal formalism revisited with wavelets, *Int. J. Bifurc. Chaos*, 4, 245–302, 1994. 778 779

- Ouzounov, D., Liu, D., Chunli, K., Cervone, G., Kafatos, M., and Taylor, P.: Outgoing long wave radiation variability from IR satellite data prior to major earthquakes, *Tectonophysics*, 431, 211–220, 2007. 780
781
- Panda, M. N., Mosher, C., and Chopra, A. K.: Application of wavelet transforms to reservoir data analysis and scaling, in: *SPE Annual Technical Conference and Exhibition*, 1996. 782
783
- Panda, S. K., Choudhury, S., Saraf, A. K., and Das, J. D.: MODIS land surface temperature data detects thermal anomaly preceding 8 October 2005 Kashmir earthquake, *Int. J. Remote Sens.*, 28, 4587–4596, 2007. 784
785
- Pastén, D. and Pavez-Orrego, C.: Multifractal time evolution for intraplate earthquakes recorded in southern Norway during 1980–2021, *Chaos, Solitons & Fractals*, 167, 113000, 2023. 786
787
788
- Prajapati, R., Arora, A.: Investigation of geomagnetic field variations in search of seismo-electromagnetic emissions associated with earthquakes in subduction zone of Andaman-Nicobar, India, *Natural Hazards and Earth System Sciences*, under review. 789
790
791
792
- Potirakis, S. M., Hayakawa, M., and Schekotov, A.: Fractal analysis of the ground-recorded ULF magnetic fields prior to the 11 March 2011 Tohoku earthquake ($M_W = 9$): discriminating possible earthquake precursors from space-sourced disturbances, *Nat. Hazards*, 85, 59–86, <https://doi.org/10.1007/s11069-016-2558-8>, 2017. 793
794
795
796
- Rahimi-Majd, M., Shirzad, T., and Najafi, M. N.: A self-organized critical model and multifractal analysis for earthquakes in Central Alborz, Iran, *Sci. Rep.*, 12, 8364, 2022. 797
798
799
- Rawat, G., Chauhan, V., and Dhamodharan, S.: Fractal dimension variability in ULF magnetic field with reference to local earthquakes at MPGO, Ghuttu, *Geomatics, Nat. Hazards Risk*, 7, 1937–1947, <https://doi.org/10.1080/19475705.2015.1137242>, 2016. 800
801
802
- Rikitake, T.: Earthquake precursors, *Bull. Seismol. Soc. Am.*, 65, 1133–1162, 1975. 803
- Scholz, C. H., Sykes, L. R., and Aggarwal, Y. P.: Earthquake Prediction: A Physical Basis: Rock dilatancy and water diffusion may explain a large class of phenomena precursory to earthquakes., *Science (80-.)*, 181, 803–810, 1973. 804
805
806
- Serrano, E. and Figliola, A.: Wavelet Leaders: A new method to estimate the multifractal singularity spectra, *Phys. A Stat. Mech. its Appl.*, 388, 2793–2805, <https://doi.org/10.1016/j.physa.2009.03.043>, 2009. 807
808
809
- Sethumadhav, M. S., Gunnell, Y., Ahmed, M. M., and Chinnaiah: Late Archean manganese mineralization and younger supergene manganese ores in the Anmod-Bisgod region, Western Dharwar Craton, southern India: Geological characterization, palaeoenvironmental history, and geomorphological setting, *Ore Geol. Rev.*, 38, 70–89, <https://doi.org/10.1016/j.oregeorev.2010.06.001>, 2010. 810
811
812
813

- Shen, Y. and Tian, B.: Bilinear auto-Bäcklund transformations and soliton solutions of a (3+ 1)-dimensional generalized nonlinear evolution equation for the shallow water waves, *Appl. Math. Lett.*, 122, 107301, 2021. 814
815
816
- Smirnova, N., Hayakawa, M., and Gotoh, K.: Precursory behavior of fractal characteristics of the ULF electromagnetic fields in seismic active zones before strong earthquakes, *Phys. Chem. Earth, Parts A/B/C*, 29, 445–451, 2004. 817
818
819
- Smirnova, N. A., Kiyashchenko, D. A., Troyan, V. N., and Hayakawa, M.: Multifractal Approach to Study the Earthquake Precursory Signatures Using the Ground-Based Observations, *Review of Applied Physics*, Hayakawa and Ida, 2013. 820
821
822
- Stanica, D. A. and Stănică, D.: ULF pre-seismic geomagnetic anomalous signal related to Mw8.1 offshore chiapas earthquake, Mexico on 8 September 2017, *Entropy*, 21, <https://doi.org/10.3390/e21010029>, 2019. 823
824
- Szczepaniak, A. and Macek, W. M.: Asymmetric multifractal model for solar wind intermittent turbulence, *Nonlinear Process. Geophys.*, 15, 615–620, 2008. 825
826
- Telesca, L., Lapenna, V., and Macchiato, M.: Multifractal fluctuations in seismic interspike series, *Phys. A Stat. Mech. its Appl.*, 354, 629–640, 2005. 827
828
829
- Turcotte, D. L.: Fractals in geology and geophysics, *Pure Appl. Geophys.*, 131, 171–196, 1989. 830
- Uyeda, S., Hayakawa, M., Nagao, T., Molchanov, O., Hattori, K., Orihara, Y., Gotoh, K., Akinaga, Y., and Tanaka, H.: Electric and magnetic phenomena observed before the volcano-seismic activity in 2000 in the Izu Island Region, Japan, *Proc. Natl. Acad. Sci.*, 99, 7352–7355, 2002. 831
832
833
- Virk, H. S., Walia, V., and Kumar, N.: Helium/radon precursory anomalies of Chamoli earthquake, Garhwal Himalaya, India, *J. Geodyn.*, 31, 201–210, 2001. 834
835
- Wendt, H.: Contributions of Wavelet Leaders and Bootstrap to Multifractal Analysis : Images , Estimation Performance , Dependence Structure and Vanishing Moments . Confidence Intervals and Hypothesis Tests, 1–292, 2008. 836
837
838
- Xu, G., Han, P., Huang, Q., Hattori, K., Febriani, F., and Yamaguchi, H.: Anomalous behaviors of geomagnetic diurnal variations prior to the 2011 off the Pacific coast of Tohoku earthquake (Mw9.0), *J. Asian Earth Sci.*, 77, 59–65, <https://doi.org/10.1016/j.jseaes.2013.08.011>, 2013. 839
840
841
842
- Yang, H., Pan, H., Wu, A., Luo, M., Konaté, A. A., and Meng, Q.: Application of well logs integration and 843

wavelet transform to improve fracture zones detection in metamorphic rocks, *J. Pet. Sci. Eng.*, 157, 716–723, 844
<https://doi.org/10.1016/j.petro.2017.07.057>, 2017. 845

846

Yen, H.-Y., Chen, C.-H., Yeh, Y.-H., Liu, J.-Y., Lin, C.-R., and Tsai, Y.-B.: Geomagnetic fluctuations during 847
the 1999 Chi-Chi earthquake in Taiwan, *Earth Planets Space*, 39–45 pp., 2004. 848

849

850

851

852

853

854

855

856

857

858

859

860